Kastamonu Uni., Orman Fakültesi Dergisi, 2018, 18 (1): 62-74 Research Article
Kastamonu Univ., Journal of Forestry Faculty
Doi: 10.17475/kastorman.409185

Investigation of mechanical behavior of wood polymer nanocomposites (WPNs) samples using static vickers microhardness tester

Elif ASIKUZUN[1]*, Alperen KAYMAKCI[2]

[1]Kastamonu University, Faculty of Engineering and Architecture, Department of Metallurgy and Material Engineering, 37100 Kastamonu, TURKEY
[2]Kastamonu University, Faculty of Forestry, Department of Forest Industry Engineering, 37100 Kastamonu, TURKEY
*Corresponding author: easikuzun@kastamonu.edu.tr

Received date: 18.01.2018 Accepted date: 23.02.2018

Abstract

Aim of study: In this study, XRD and Vickers microhardness analyses of wood polymer nanocomposites (WPNs) materials are carried out in detail. Especially, we are focused on the mechanical analysis.

Area of study: Pine wood flour (40 mesh) as lignocellulosic filler obtained from a commercial WPC manufacturer (sema wood) in Tekirdag, Turkey are used.

Material and Methods: Polypropylene, nano TiO_2 and coupling agent are used in the experiments. Depending on the nanocomposite groups, granulated polymer, wood flour, nano TiO_2 and MAPP are mixed. Then this mixture is compounded in a laboratory scale twin-screw extruder at 40 rpm screw speed.

Main results: According to the obtained hardness results, all of the materials show RISE (Reverse Indentation Size Effect) behavior. Experimental microhardness results are compared with the mathematical models (Meyer's law, Proportional sample Resistance (PSR), Elastic/Plastic Deformation (EPD) and Indentation-Induced Cracking (IIC) models) used in the microhardness analysis of materials in the literature and the most suitable model for microhardness values of materials was determined. According to the models, IIC model is the most suitable to determine the micromechanical properties.

Research highlights: Structural and mechanical properties of WPNs materials are investigated. The increase in the microhardness values of the all sample depends on the increase of applied load. In addition, the microhardness values decrease with increased TiO_2 concentration in the samples and microhardness values reach a saturation region at around 1.5 N for the samples.

Keywords: WPNs, Vickers microhardness, IIC model, RISE, XRD

Ahşap polimer nanokompozit (WPN) numunelerinin mekanik davranışlarının statik vickers mikro sertlik test cihazı kullanılarak incelenmesi

Özet

Çalışmanın amacı: Bu çalışmada, ahşap polimer nanokompozit (WPN) malzemelerinin XRD ve Vickers mikrosertlik analizleri detaylı bir şekilde gerçekleştirilmiştir. Özellikle mekanik analizler üzerine odaklanılmıştır.

Çalışma alanı: Tekirdağ'da ticari bir WPC üreticisinden (Sema Ahşap) elde edilen lignoselülozik dolgu maddesi olarak çam kerestesi kullanılmıştır.

Materyal ve Yöntem: Deneylerde polipropilen, nano TiO_2 ve birleştirme maddesi kullanılmıştır. Nanokompozit gruplara bağlı olarak, granül haline getirilmiş polimer, odun unu, nano TiO2 ve MAPP karıştırılmıştır. Daha sonra bu karışım, 40 rpm'lik vida hızında laboratuar ölçekli çift vidalı bir ekstrüderde birleştirilmiştir.

Temel Sonuçlar: Elde edilen sertlik sonuçlarına göre, tüm materyaller RISE (Ters Çentik Boyutu Etkisi) davranışını göstermektedir. Deneysel sonuçlar, literatürde malzemelerin mikrosertlik analizlerinde kullanılan matematiksel modeller (Meyer Kanunu, Orantılı Numune Direnci (PSR), Elastik/Plastik Deformasyon (EPD) ve Çentici Kaynaklı Yarılma (IIC) modelleri ile karşılaştırılmış ve en uygun model belirlenmiştir. Bu modellere göre, IIC modeli, malzemelerin mikromekanik özelliklerini belirlemek için en uygun modeldir.

Araştırma vurguları: WPN'lerin yapısal ve mekanik özellikleri araştırılmıştır. Tüm numunenin mikrosertlik değerlerindeki artış uygulanan yükün artmasına bağlıdır. Ek olarak, numunelerde TiO_2 konsantrasyonun artması ile mikrosertlik değerleri azalmakta ve yaklaşık 1.5 N'de doyma bölgesine ulaşmaktadır.

Anahtar kelimeler: WPN, Vickers mikrosertlik, IIC modeli, RISE, XRD

Introduction

Wood is one of the most important renewable structural material in the world. Wood material is effectively used in many areas due to its durability and natural beauty. Nevertheless, however, some disadvantages such as high moisture absorption, biological degradation and physical and mechanical properties which change with environmental variations that wood has shown are limiting its use area (Piccardo and Magliocco, 2013; Okoh, 2014). Various methods have been developed to eliminate the negative characteristics of the wood. Wood modification using appropriate chemical treatments, such as the formation of wood polymer composites (WPCs), has shown some potential in improving wood properties (Ozmen et al., 2013; Cetin et al., 2015; Kaymakci et al., 2017). Many chemicals such as styrene, epoxy resin, urethane, phenol formaldehyde resin, urea formaldehyde resin, methyl methacrylate, vinyl, and acrylic monomer are widely used for the improvement of wood properties.

Wood based composite products such as wood polymer composites, particleboard, Medium density fiberboard (MDF) and plywood are generally used in panel furniture production in the furniture industry in the world. But factors such as the reduction of natural raw material resources, the development of environmental awareness, the development of new production technologies, and the difficulty of global competition make furniture manufacturers think that new materials should be used. Because of this situation, the wood based composite manufacturers have been directed to search for alternative raw materials and novel manufacturing methods.

The composite can be defined as a new product resulting in a physical mixture of multiple components. Thus, the two materials in the different properties can form a new material complementing each other. In order to improve the mechanical properties of polymer composites, many different lignocellulosic and mineral based fillers and reinforcing materials with different properties are used. Wood plastic composites are used in exterior coating materials, in room panes, windows and door frames, automobile interior parts and many other products.

Nanotechnology is primarily used in medicine, biotechnology, medicine, materials, electronics, defense, textile, automotive, construction, energy and so on. Various researches are continuing in the direction of using them in the fields. However, the use of nanotechnology in the forest products industry is quite new. In nanocomposites, at least one dimension of the fillers is in the order of nanometers. Various nanomaterials such as carbon nanotubes, SiO_2, MgO, boron nitrides and TiO_2 are evaluated in the production of polymer nanocomposites as filler. The use of nano fillers in nanocomposite production significantly improves the physical, mechanical, thermal and optical properties of the composite materials (Candan and Akbulut, 2013).

According to most nanocomposite researchers, TiO_2 nano filler is increasingly being investigated because of high specific properties such as non-toxic, chemically inert, low cost, corrosion resistant and has a high refractive index and high hardness. Literature has also demonstrated that nanoscale TiO_2 reinforcement brings attractive properties attained at very low TiO_2 content, which make polymer TiO_2 nanocomposites a promising new class of materials (Farhoodi et al., 2012; Ahmed et al., 2016; Deka and Maji, 2011).

The process of preparing a polymer nanocomposite involves the blending of polymer and nano materials in a manner that nano materials are distributed homogeneously throughout the polymer matrix. The success of a polymer nanocomposite related within the degree of cooperation of individual nano materials within the polymer matrix, which is directly proportional to the total surface area between the nano materials and the polymer. The more contact area between the nano materials and the polymer matrix resulted extraordinary mechanical, thermal and electronic properties of nano materials in the resulting composite.

There are a lot of studies on the effects of nanofiller such as nanoclay, graphene, silicon dioxide (SiO_2), and carbon nanotube on the

mechanical performance of wood polymer composites. However, the hardness and crystallinity of the wood polymer composites containing titanium dioxide (TiO_2) were not extensively investigated. Also combination of wood flour and TiO_2 on properties wood polymer nanocomposites (WPNs) is aroused interest by wood composite scientist. For this reason, this study focused on the effect of TiO_2 on the mechanical and crystallinity properties of wood polymer nanocomposites (WPNs).

The behavior of a material under a specific load depends on the mechanical properties of the material (Şahin et al., 2007; Sangwal, 2002; Graaf, 2004; Lopesa, 2011). Mechanical properties vary according to the type of applied load. Generally, there are two different load types as static and dynamic. The various mechanical properties of materials are determined depending on the load type applied. For example, fatigue toughness is one of important properties of the materials and is identified by the behavior of the material under applied dynamic load. Other material properties such as tensile strength, yield strength, fracture toughness, toughness, ductility, elastic modulus and hardness are determined by the behavior of the material under applied static load (Tosun et al., 2014; Ozturk et al., 2014; Arda et al., 2013).

There are many test methods are used to determine the mechanical properties of materials. The most common static load test methods are the tensile, compression, torsion, bending, hardness and creep tests. The most common dynamic load test methods are the fatigue test and notch impact test.

The aim of this study is investigation of micromechanical and microstructural properties of materials. The X-ray Diffractometer (XRD) are used to determination of structural properties and Vickers microhardness measurements are used to determination of micromechanic properties of materials. These measurements and obtained results are given in the Result and Discussions.

Material and Method

Polypropylene (Borealis Incorp), nano TiO_2 (Grafen company), and coupling agent (Optim-425, MFI/190°C; 2,16 kg = 120 g/10 min, density: 0,91 g/cm^3) are used in the experiments. Some physical and technic properties of nano TiO_2 are presented in Table 1.

Table 1. Specification of the TiO_2

Properties	TiO_2
Apperance	White Powder
Average Particle Size	10-25 nm
Purity	99.5 %
Surface Area	> 50 m^2/g

Pine wood flour (40 mesh) as lignocellulosic filler obtained from a commercial WPC manufacturer (sema wood) in Tekirdag, Turkey. Experimental design of the study is presented in Table 2.

Table 2. Experimental design of the study

WPN Groups	Polypropylene (wt%)	Pine Wood Flour (wt%)	TiO_2 (wt%)	MAPP (wt%)
A	50	50	0	3
B	50	50	1	3
C	50	50	2	3
D	50	50	3	3
E	50	50	4	3
F	50	50	5	3

Depending on the nanocomposite groups, granulated polymer, wood flour, nano TiO_2 and MAPP are mixed. Then this mixture is compounded in a laboratory scale twin-screw extruder at 40 rpm screw speed. Extruder temperatures are set as 170, 180, 185, 190, and 200 °C for 5 heating zones. The extrudates are collected, cooled and granulated into pellets. Finally, pellets are injected at injection pressure between 5 and 6 MPa with cooling time about 30 s. The specimens are conditioned at a temperature of 23 °C and relative humidity of 50%.

Result and Discussion

XRD Measurements

X-ray Diffraction measurements were performed by Bruker D8 Advance X-ray powder diffractometer device using Cu Kα radiation source (λ= 0,154 nm). Scanning

rate and scan speed were 4° ≤ 2Θ ≤ 45° and 2°/min, respectively. The XRD analyses of samples are shown in Figure 1. The XRD graph (Fig. 1) evidently shows that all diffractograms exhibited sharp peaks between $2\theta = 14°$-22°. The crystalline peak intensity of the polymer nanocomposites appeared in the range of 2θ = 14–22° is not change with the increase in the level of incorporation of TiO_2. However, the intensities of peak nanoparticles is not significantly changed with higher concentration of TiO_2 in the composite. This indicates that the crystal structure of polymer is preserved with TiO_2 concentration.

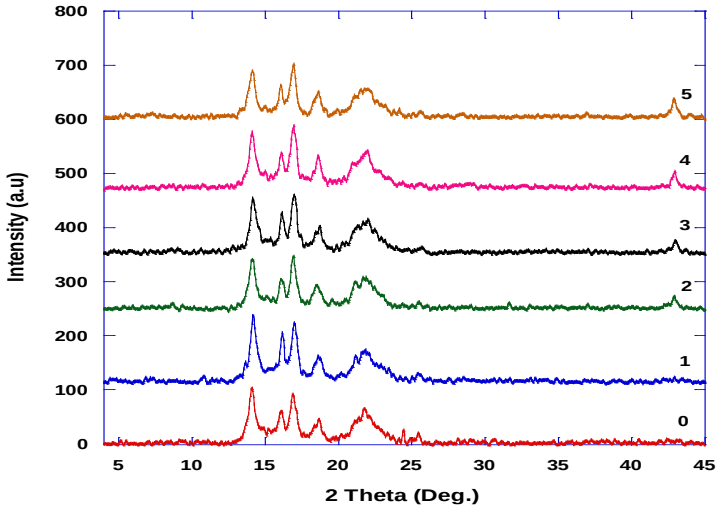

Figure 1. XRD patterns of all samples

Vickers Microhardness Measurements

Vickers hardness test is developed to measure the hardness of materials. It can be used for all materials and has one of the broadest scales among hardness tests. Hardness is determined when force is applied by an indenter to the surface area. In our study, the hardness unit is taken as GPa.

In this study, the mechanical characterizations of nanocomposites materials are performed using Shimadzu brand HMV-2 model digital microhardness tester. The Vickers microhardness values (H_v) of different applied loadings in the range of 0.245– 2.940 N for 10 s can be calculated using Eqn.1. This process is repeated five times and average value of hardness is found. F is applied load on the surface of the material. A is the surface area in terms of micrometers square.

$$H_v = F/A \approx \frac{1854.4\,F}{d^2} \quad GPa \qquad (1)$$

The change of the load dependent microhardness values as a function of the test loads are shown in Figure 2 in detail.

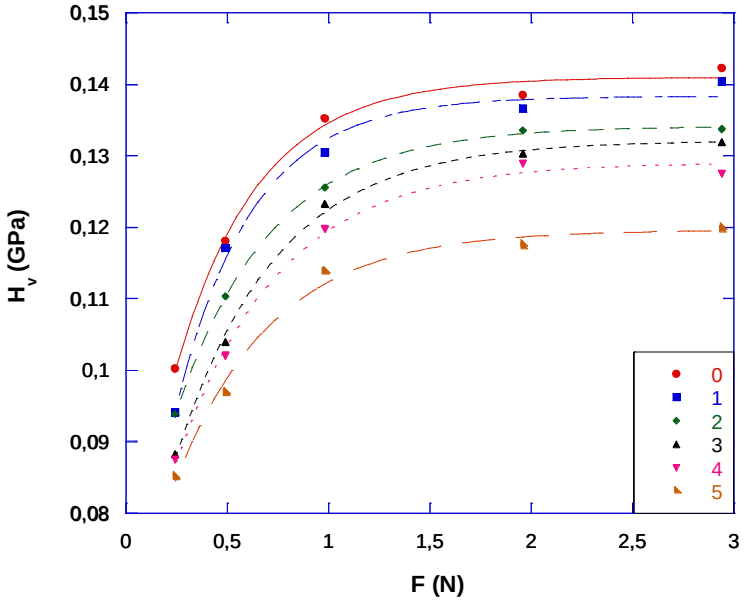

Figure 2. The variations of microhardness with load for the samples

It can be seen from figure that the microhardness values decrease with increased TiO_2 concentration in the samples. Microhardness values of all samples are given in Table 3. In addition, microhardness values reach a saturation region at around 1.5 N for the samples. The hardness value of the sample observed RISE behavior depends on the applied load. It shows that the indenter size is associated with applied load. This nonlinear case is named as Reverse Indentation Size Effect (RISE) in the literature (Gong et al., 1999; Elmustafa and Stone, 2003). Smaller indentation load shows a smaller hardness value. In addition, optical trace photos of the indentations for each sample under 0490 N $(50g)$ load are shown in Figure 3.

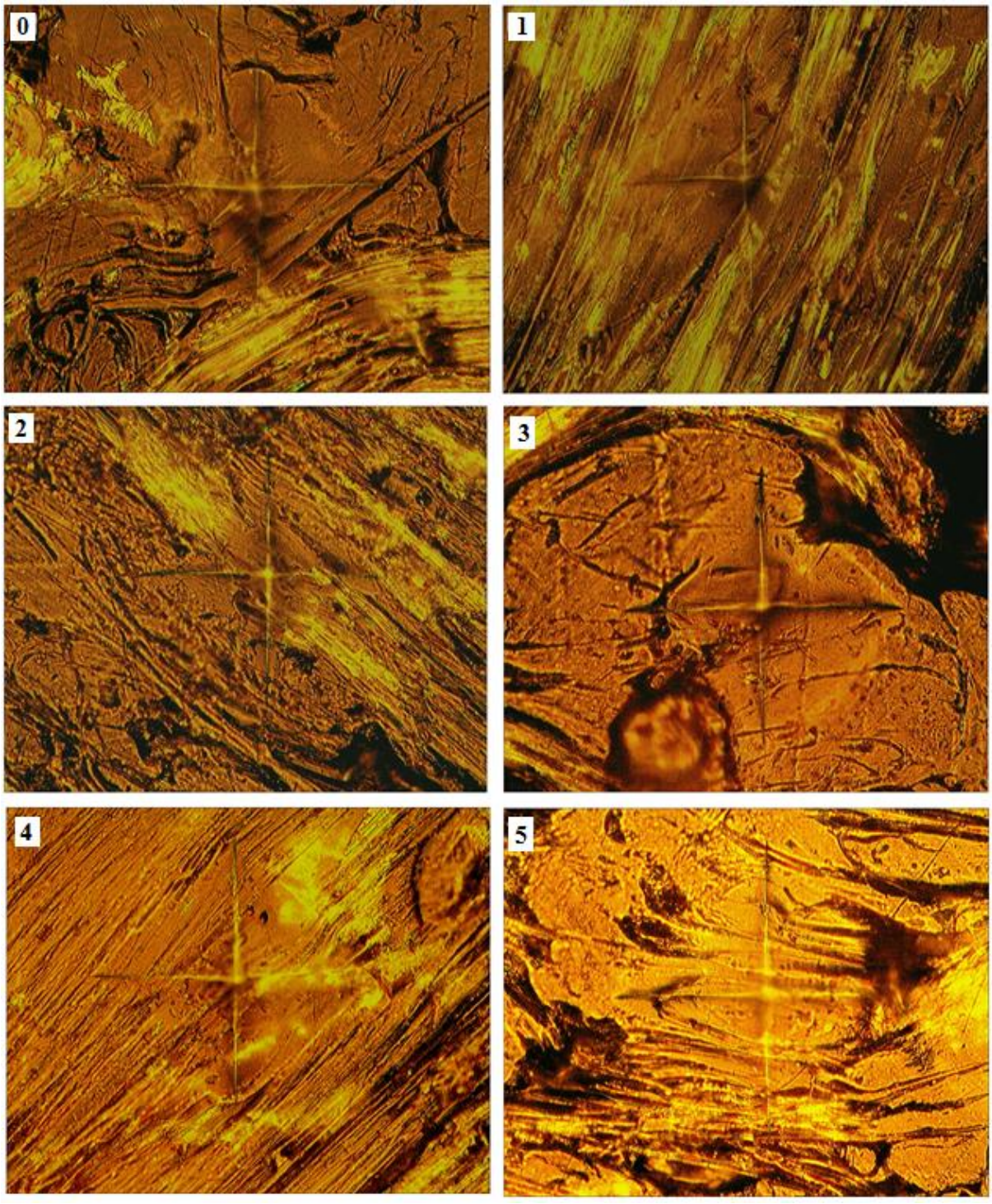

Figure 3. The optical trace photos under 0.490 N load for the samples

Table 3. The calculated load dependent H_v for the samples

Samples	F (N)	H_V (GPa)	H_v (GPa) (in plateau region)	Samples	F (N)	H_V (GPa)	H_v (GPa) (in plateau region)
0	0.245	0.100	0.138-0.142	3	0.245	0.088	0.130-0.131
	0.490	0.118			0.490	0.103	
	0.980	0.135			0.980	0.123	
	1.960	0.138			1.960	0.130	
	2.940	0.142			2.940	0.131	
1	0.245	0.094	0.136-0.140	4	0.245	0.087	0.128-0.127
	0.490	0.117			0.490	0.101	
	0.980	0.130			0.980	0.119	
	1.960	0.136			1.960	0.128	
	2.940	0.140			2.940	0.127	
2	0.245	0.093	0.133-0.134	5	0.245	0.085	0.117-0.119
	0.490	0.110			0.490	0.096	
	0.980	0.125			0.980	0.113	
	1.960	0.133			1.960	0.117	
	2.940	0.134			2.940	0.119	

More detailed analysis is made using data obtained from all results regarding microhardness of materials that have *RISE* behavior. Therefore, the different models are presented in order to explain the behavior of materials in the literature (Arda et al., 2013; Kölemen et al., 2006; Sahin et al., 2008). In this section, the comparisons are relevant to hardness are made using the Meyer Law, the proportional sample resistance (*PSR)*, the elastic/plastic deformation (*EPD)* and indentation induced cracking (*IIC)* models. These models are load independent microhardness models. Analyses on these models are given below.

Meyer's Law

Meyer's law which is an expression of simple experimental is developed to explain of *ISE* (Indentation Size Effect) or *RISE* (Reverse Indentation Size Effect) behavior of materials (Tosun et al., 2014).

$$F = Kd^n \qquad (II)$$

Meyer number *n* is a measure of *ISE or RISE*. If the *n* value is greater than *2*, *RISE* behavior is obtained. If the *n* value is less than *2*, *ISE* behavior is obtained (Quinn and Quinn, 1997; Ozturk et al., 2011; Cetinkara et al., 2009). Obtained results are shown in Table 4. As shown in table, *n* values of the all samples are greater than 2. As a result, according to results of Meyer's Law (Figure 4), all samples show *RISE* behavior.

Table 4. Best-fit results of experimental data according to Meyer's law

Samples	Meyer number n_k	InK (GPa)
0	2.31	-11.08
1	2.35	-11.29
2	2.33	-11.24
3	2.38	-11.56
4	2.37	-11.50

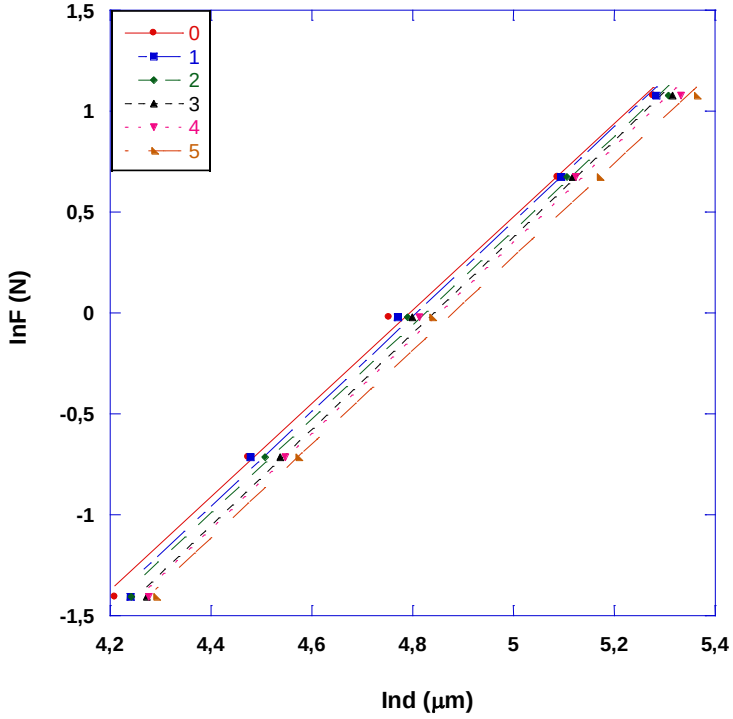

Proportional Sample Resistance (PSR) Model

According to *PSR* model, the $F/d - d$ graphs of the samples are given in Figure 5. It can be seen from Table 5, the α constant that is the value where $(F/d) - d$ axis intersected (Eqn.III) of all the samples shows only negative values. This result confirms that the character of the displacement of these materials is in the form of the *RISE* behavior. This situation confirms that the plastic deformations occur in these samples which show the *RISE* behavior.

$$F/d = \alpha + \beta d \qquad (III)$$

In this model, load–independent hardness values are calculated with the Eqn. (IV).

$$H_{PSR} = 1854.4\beta \qquad (IV)$$

Quinn and Quinn (1997) show that there is a transition region to plateau where hardness remains unchanged after from a certain of load value in hardness-load change curves. They indicate that the hardness value corresponds to hardness in this region is called as the plateau region is true hardness. When H_v values of samples are analyzed (Table 3), it is shown that hardness reached to plateau region after 1.5 N. If H_{PSR} hardness values are compared with value that corresponds to the plateau region, it can be seen clearly that these microhardness values are quite far from the plateau region (Table 5). Therefore, it is apparent that the *PSR* model is unsuccessful to determine the real hardness values of the materials

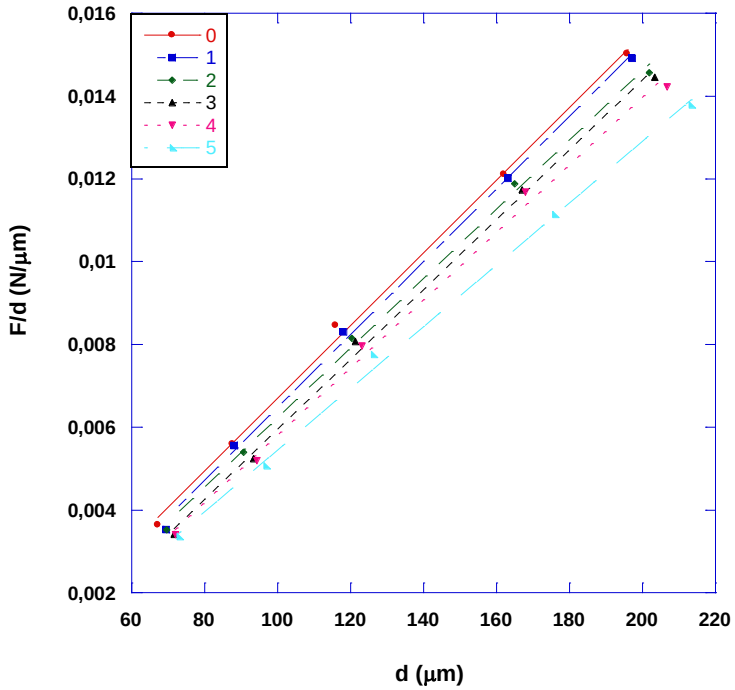

Figure 5. Plots of F/*d* versus *d* for the samples

Table 5. Best-fit results of experimental data according to PSR model

Samples	α x10 $^{-3}$ (N)	β x10 $^{-5}$ (N/µm)	H_{PRS} (GPa)	H_V (GPa) (in plateau region)
0	-2.09	8.78	0.162	0.138-0.142
1	-2.31	8.79	0.163	0.136-0.140
2	-2.16	8.39	0.155	0.133-0.134
3	-2.51	8.45	0.156	0.130-0.131
4	-2.35	8.16	0.151	0.128-0.127
5	-2.00	7.45	0.138	0.117-0.119

Elastic/Plastic Deformation (EPD) Model

According to the elastic/plastic deformation model (EPD), the relationship between the applied load and trace is given in the following Eqn. (5) (Bull et al., 1989; Upit and Varchenya, 1966).

$$F = A_2(d_p + d_e) \quad (5)$$

Where A_2 is a constant, d_e is related to the plastic deformation (d_p). A_2 and d_e values can be calculated from graph of $F^{1/2} - dp$ (Fig.6). In this model, load independent microhardness value is calculated from Eqn.6.

$$H_{EPD} = 1854.4A_2 \quad (6)$$

When this model is applied, as seen in Table 6, d_e value found from the point where the graph intersects the y axis is negative for all samples. Because there is no elastic deformation for the applied loads. This result is evidence of the RISE behavior of the material.

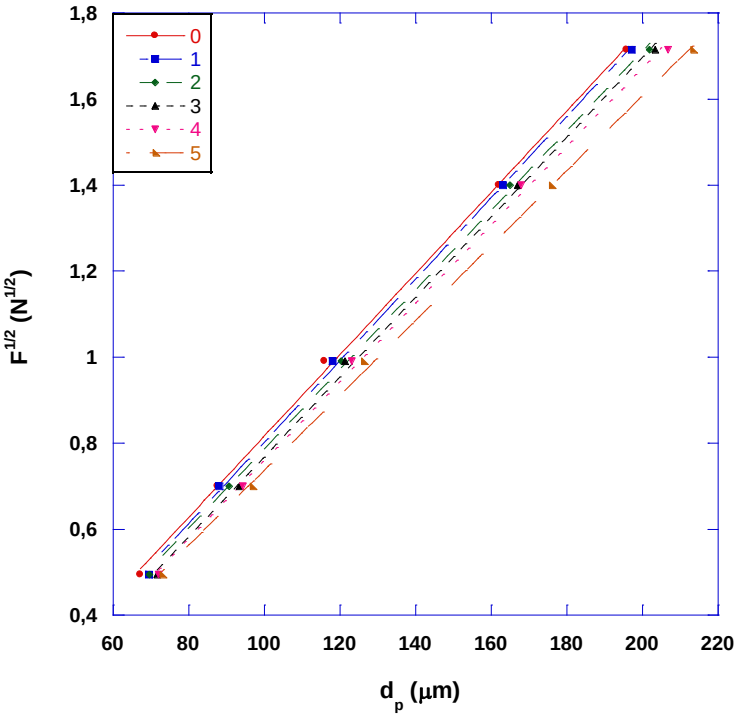

Figure 6. Plots of diagonal length versus square root of applied loads for the samples

Microhardness values that are calculated by EPD model are so far from plateau region (Table 6). As a result, it is clearly observed that EPD model is not successful to determine the microhardness of the samples.

Table 6. Best-fit results of experimental data according to EPD model

Samples	$A_2^{1/2}$ (GPa)	d_e (µm)	H_{EDP} (GPa)	H_V (GPa)
0	0.00944	-0.12	0.165	0.138-0.142
1	0.00946	-0.14	0.165	0.136-0.140
2	0.00923	-0.13	0.157	0.133-0.134
3	0.00929	-0.16	0.160	0.130-0.131
4	0.00912	-0.15	0.154	0.128-0.127
5	0.00870	-0.13	0.140	0.117-0.119

Indentation-Induced Cracking (IIC) Model

IIC model is developed to explain the *RISE* behavior in the samples (Li and Bradt, 1996). According to the model, the applied test load is offset by the total resistance of the sample at maximum depth. According to this model, while the friction and elastic effects led to normal *ISE* behavior, indentation cracks led to RISE behavior. Li and Bradt reported the importance of the elastic and frictional effects in the PSR model. Microhardness values calculated by this model is given by,

$$H_v = \lambda_1 K_1 \left(\frac{F}{d^2}\right) + K_2 \left(\frac{F^{\frac{5}{3}}}{d^3}\right) \quad (7)$$

is given by the equation. Here, d is the trace's diameter and λ_1, K_1 and K_2 are constants. While, K_2 value is dependent on the applied load, K_1 value is dependent on the geometry of the indenter.

While, $H_v=K_1(F/d^2)$, $\lambda_1=1$ and $K_2(F^{5/3}/d^3)=0$ for ideal plastic materials, $H_v=K_2\ (F^{5/3}/d^3)$ and $\lambda_1=0$ for ideal brittle solids. If the investigated material is a brittle material only second part of the equation is used,

$$H_v = K\left(\frac{F^{\frac{5}{3}}}{d^3}\right)^m \quad (8)$$

Values of K and m are load independent constants and are obtained from the $In(H_v)$-$In(F^{5/3}/d^3)$ graph (Fig. 7). m is used to determine the *ISE* or the *RISE* behaviors. If m>0.6 the material shows a normal *ISE* behavior, however if m<0.6 the material shows *RISE* behavior (Awad et al., 2011). These values are given in the Table 7.

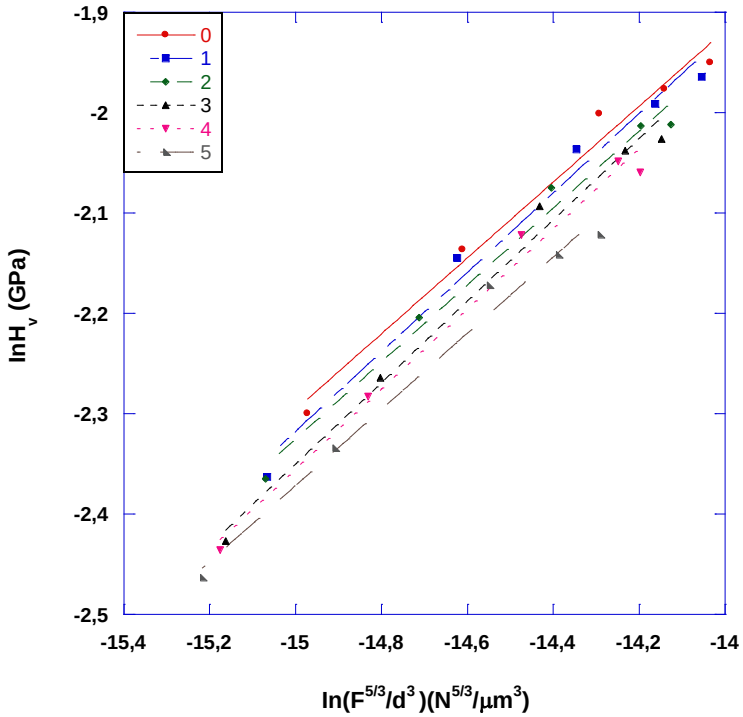

Figure 7. Variation of from $In(Hv)$ with $In(F^{5/3}/d^3)$ according to IIC model

Analyzing data in Table 7, it can be seen that *IIC* model hardness values are close to the hardness values of the sample. This result confirms that only plastic deformation is observed in the samples. As can be seen from the table 8, *IIC* model is the most appropriate model for all other samples showing *RISE* behavior (Asikuzun et al., 2015).

Table 7. Best-fit results of experimental data according to *IIC* model

Samples	m	InK ($N^{(3-5m)/3}/\mu m^{(2-3m)}$)	H_{IIC} (GPa)	H_V (GPa)
0	0.372	3.37	0.141	0.138-0.142
1	0.395	3.62	0.134	0.136-0.140
2	0.383	3.42	0.124	0.133-0.134
3	0.405	3.72	0.123	0.130-0.131
4	0.410	3.63	0.128	0.128-0.127
5	0.37	3.31	0.121	0.117-0.119

Table 8. The results of load dependent Vickers microhardness at the plateau region and load independent hardness values calculated using *PSR*, *EPD* and *IIC* models

Samples	H_{EDP} (GPa)	H_{PRS} (GPa)	H_{IIC} (GPa)	H_V (GPa)
0	0.165	0.162	0.141	0.138-0.142
1	0.165	0.163	0.134	0.136-0.140
2	0.157	0.155	0.124	0.133-0.134
3	0.160	0.156	0.123	0.130-0.131
4	0.154	0.151	0.128	0.128-0.127
5	0.140	0.138	0.121	0.117-0.119

Conclusion

In this section, the results of microhardness measurements of wood polymer nanocomposites are reported. The increase in the microhardness values of the all sample depends on the increase of applied load, which shows *RISE* behavior. In addition, the microhardness values decrease with increased TiO_2 concentration in the samples and microhardness values reach a saturation region at around 1.5 N for the samples. Among the applied models, the IIC model is identified as the most suitable model for Vickers microhardness analysis of wood polymer nanocomposites.

References

Awad, R., Abou Aly, A. I., Kamal, M., Anas, M. (2011). Mechanical Properties of $(Cu_{0.5}Tl_{0.5})$-1223 Substituted by Pr. *J. Supercond. Nov. Magn., 24,* 1947-1956.

Arda, L., Ozturk, O., Asikuzun, E., Ataoglu, S. (2013). Structural and mechanical properties of transition metals doped ZnMgO nanoparticles. *Powder Technology, 235,* 479-484.

Asikuzun, E., Ozturk, O., L., Arda, Akcan, D., Senol, S.D., Terzioglu, C. (2015). Preparation, structural and micromechanical properties of (Al/Mg) co-doped ZnO nanoparticles by sol–gel process. *J. Mat. Sci.: in Elect. 26,* 8147–8159.

Ahmed, M.A., El-Shennawy, M., Althomali, Y.M., Omar, A.A. (2016). Effect of Titanium Dioxide Nano Particles Incorporation on Mechanical and Physical Properties on Two Different Types of Acrylic Resin Denture Base. *World Journal of Nano Science and Engineering, 6*, 111-119.

Bull, S.J., Page,T.F., Yoffe, E.H. (1989). An explanation of the indentation size effect in ceramics. *Philosophical Magazine Letters, 59,* 281-288.

Cetinkara, H.A., Yilmazlar, M., Ozturk, O., Nursoy, M., Terzioglu, C. (2009). The influence of cooling rates on microstructure and mechanical properties of $Bi_{1.6}Pb_{0.4}Sr_2Ca_2Cu_3O_y$ superconductors. *In Journal of Physics: Conference Series 153,* 012038.

Candan, Z., Akbulut, T. (2013). Developing environmentally friendly wood composite panels by nanotechnology. *BioResources, 8 (3)*, 3590-3598.

Cetin, N., Cetin, N., Harper, D. (2015). Vinyl acetate-modified microcrystalline cellulose-reinforced HDPE composites prepared by twin-screw extrusion. *Turkish Journal of Agriculture and Forestry, 39 (1),* 39-47.

Deka, B.K., Maji, T.K. (2011). Effect of TiO2 and nanoclay on the properties of wood polymer nanocomposites. *Composites Part A: Applied Science and Manufacturing, 42 (12),* 2117-2125.

Elmustafa, A.A., Stone, D.S. (2003). Nanoindentation and the indentation size effect: Kinetics of deformation and strain gradient plasticity. *Journal of the Mechanics and Physics of Solids, 51(2),* 357-381.

Farhoodi, M., Dadashi, S., Mousavi, S.M.A., Sotudeh-Gharebagh, R., Emam-Djomeh, Z., Oromiehie, A., Hemmati, F. (2012). Influence of TiO2 Nanoparticle Filler on the Properties of PET and PLA

Nanocomposites. *Polymer (Korea), 36 (6)*,745-755.

Gong, J., Wu, J., Guan, Z. (1999). Examination of the indentation size effect in low-load Vickers hardness testing of ceramics. *Journal of the European Ceramic Society, 19(15),* 2625-2631.

Graaf, D.D., Braciszewicz, M., Hintzen, H.T., Sopicka-Lizer, M., De With, G. (2004). The Influence of The Composition on (The Load-Dependence of) The Microhardness of Y–;Si–;Al–;O–;N Glasses As Measured By Vickers Indentation. *J. Mater. Sci., 39*, 2145.

Kölemen, U., Uzun, O., Yılmazlar, M., Güçlü, N., Yanmaz, E. (2006). Hardness and microstructural analysis of $Bi_{1.6}Pb_{0.4}Sr_2Ca_{2-x}Sm_xCu_3O_y$ polycrystalline superconductors. *Journal of alloys and compounds, 415(1),* 300-306.

Kaymakci, A., Gulec, T., Hosseinihashemi, S.K., Ayrilmis, N. (2017). Physical, Mechanical and Thermal Properties of Wood/ Zeolıte/Plastic Hybrid Composites, Maderas. *Ciencia y tecnología, 19 (3)*, 339–348.

Li, H., Bradt, R.C. (1996). The effect of indentation-induced cracking on the apparent microhardness. *J. Mater. Sci., 31,* 1065–1070.

Lopesa, E.S.N., Cremascoa, A., Afonsob, C.R.M., Caram, R. (2011). Effects of double aging heat treatment on the microstructure, Vickers hardness and elastic modulus of Ti–Nb alloys. *Materials Characterization, 62,* 673-680.

Ozturk, O., Cetinkara, H.A., Asikuzun, E., Akdogan, M., Yilmazlar, M., Terzioglu, C. (2011). Investigation of mechanical and superconducting properties of iron diffusion-doped Bi-2223 superconductors. *Journal of Materials Science: Materials in Electronics, 22(9),* 1501-1508.

Ozmen, N., Cetin, N.S., Mengeloglu, F., Birinci, E., Karakus K.K. (2013). Effect of Wood Acetylation with Vinyl Acetate and Acetic Anhydride on the Properties of Wood-Plastic Composites. *Bioresources, 8 (1),* 753-767.

Ozturk, O., Asikuzun, E., and Yildirim, G. (2013). The role of Lu doping on microstructural and superconducting properties of $Bi_2Sr_2CaLu_xCu_2O_y$ superconducting system. *J. Mat. Sci.: in Elect., 24,* 1274-1281.

Okoh, E.T. (2014). Water Absorption Properties of Some Tropical Timber Species. *Journal of Energy and Natural Resources, 3 (2)*, 20-24.

Piccardo, C., Magliocco, A. (2013). The Environmental Profile of Wood in the Building Industry Today: Comments on the Results of Some LCA Studies. *American Journal of Civil Engineering and Architecture*, *1(6)*, 122-128.

Quinn, J.B., Quinn D.G. (1997). Indentation brittleness of ceramics: a fresh approach. *Journal of Materials Science, 32(16),* 4331-4346.

Sangwal, K., Surowska, B., Blaziak, P. (2002). Analysis Of The Indentatıon Size Effect In The Microhardness Measurement of Some Cobalt-Based Alloys. *Mater. Chem. Phys.*, *77,* 511.

Sahin, O., Uzun, O., Kölemen, U., Uçar, N. (2007). Dynamic Hardness And Reduced Modulus Determination On The (001) Face Of B-Sn Single Crystals By A Depth Sensing Indentation Technique. *J. Phys. Condens. Matter., 19*, 306001.

Sahin, O., Uzun, O., Sopicka-Lizer, M., Gocmez, H., Kölemen, U. (2008). Dynamic hardness and elastic modulus calculation of porous SiAlON ceramics using depth-sensing indentation technique. *Journal of the European Ceramic Society, 28(6),* 1235-1242.

Tosun, M., Ataoglu, S., Arda, L., Ozturk, O., Asikuzun, E., Akcan, D., Cakiroglu, O. (2014). Structural and mechanical properties of ZnMgO nanoparticles. *Materials Science and Engineering: A, 590,* 416-422.

Upit, G.P., Varchenya, S.A. (1966). Microhardness of alkali halide crystals. *Physica Status Solidi (b), 17(2),* 831–835.